JCTC Journal of Chemical Theory and Computation

Article

pubs.acs.org/JCTC

# Scalar Relativistic Calculations of Hyperfine Coupling Constants Using *Ab Initio* Density Matrix Renormalization Group Method in Combination with Third-Order Douglas–Kroll–Hess Transformation: Case Studies on 4d Transition Metals

Tran Nguyen Lan,*[,†,▽] Yuki Kurashige,[†,‡,§] and Takeshi Yanai[†,‡]

[†]The Graduate University for Advanced Studies, Myodaiji, Okazaki, Aichi 444-8585, Japan

[‡]Department of Theoretical and Computational Molecular Science, Institute for Molecular Science, Okazaki, Aichi 444-8585, Japan

[§]Japan Science and Technology Agency, PRESTO, 4-1-8 Honcho, Kawaguchi, Saitama 332-0012, Japan

**ABSTRACT:** We have developed a new computational scheme for high-accuracy prediction of the isotropic hyperfine coupling constant (HFCC) of heavy molecules, accounting for the high-level electron correlation effects, as well as the scalar-relativistic effects. For electron correlation, we employed the *ab initio* density matrix renormalization group (DMRG) method in conjunction with a complete active space model. The orbital-optimization procedure was employed to obtain the optimized orbitals required for accurately determining the isotropic HFCC. For the scalar-relativistic effects, we initially derived and implemented the Douglas–Kroll–Hess (DKH) hyperfine coupling operators up to the third order (DKH3) by using the direct transformation scheme. A set of 4d transition-metal radicals consisting of Ag atom, PdH, and $RhH_2$ were chosen as test cases. Good agreement between the isotropic HFCC values obtained from DMRG/DKH3 and experiment was archived. Because there are no available gas-phase values for PdH and $RhH_2$ radicals in the literature, the results from the present high-level theory may serve as benchmark data.

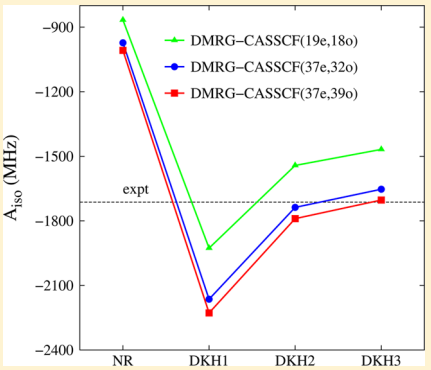


## 1. INTRODUCTION

The hyperfine coupling constants (HFCCs) play a key role in describing electron paramagnetic resonance (EPR) spectra. The HFCCs arise from the interaction between electron spin (**s**) and nuclear spin (**I**) and include both isotropic and anisotropic contributions. The isotropic HFCC is directly associated with the spin density in the vicinity of the nuclei. This leads to numerical difficulties with accurate prediction of HFCCs. Therefore, high-level methods that include electron correlations and relativity are often required to reliably predict HFCCs, especially for molecules containing heavy elements.

In the nonrelativistic (NR) limit, Bartlett and co-workers developed several approaches based on the coupled cluster (CC) method to evaluate HFCCs, including finite-field CC[1] and analytical derivative CC.[2] Momose et al.[3,4] employed the symmetry-adapted cluster-configuration interaction (SAC–CI) method to evaluate the HFCCs of several organic radicals. Chipman systematically assessed the influence of excitation levels of the configuration interaction (CI) method for the treatment of HFCCs for the CH radical,[5] and found a nonmonotonic variation of the isotropic HFCC value for the C center with increasing CI excitation level. Engels[6,7] developed a new selection procedure for the multireference CI (MRCI) method to accurately characterize HFCCs of small molecules. Density functional theory (DFT) has also been extensively used to calculate HFCCs. Among the functionals tested, hybrid functionals such as B3LYP[8,9] and PBE0[10,11] are known to perform best in many cases. In a recent assessment of DFT performance, Kossmann et al.[12] has shown that the meta-GGA functional TPSS[13] (and its hybrid version TPSSh[13]) and the double hybrid functional B2PLYP[14] generate HFCCs in acceptable agreement with experimental results.

Regarding relativity, because the isotropic HFCC depends on the spin distribution in the close vicinity of nuclei, scalar relativistic (SR) effects are prominent. The spin–orbit coupling (SOC) effects on HFCCs are often small and can be neglected in most situations. In the framework of the four-component approach (4c), Quiney and Belanzoni[15] have employed the Dirac–Hartree–Fock (DHF) approximation to calculate the HFCCs of diatomic molecules. More recently, multiconfiguration Dirac–Fock (MCDF) calculations have been carried out by Song et al.[16] for coinage atoms. Malkin and co-workers[17] have recently implemented the 4c-DFT method, including finite nuclear (FN) effects for the calculation of HFCCs. There is no doubt that the 4c level of relativistic treatment can provide accurate HFCCs. However, it is too expensive when combined with a high level of correlation treatment. Thus, the quasi-relativistic approaches formulated with the two-component (2c) wave function have become a useful tool for HFCC

**Received:** August 27, 2014

   dx.doi.org/10.1021/ct5007778 | *J. Chem. Theory Comput.* XXXX, XXX, XXX–XXX

calculations. Since the first work conducted by van Lenthe and colleagues,[18] the zeroth-order regular approximation (ZORA) based on the DFT method has been widely used.[19−22] Autschbach[23] showed that hyperfine coupling integrals calculated for atomic *s* orbitals at the ZORA level, which generally yield the largest contributions to the isotropic HFCC, are in excellent agreement with those at the 4c level for valence orbitals (not for core orbitals) of heavy elements. Implementation of the second-order Douglas−Kroll−Hess (DKH2) transformation for HFCCs was first presented by Malkin and co-workers.[24,25] Recently, Sandhoefer and colleagues[26] have successfully applied the DKH2 transformation in combination with the orbital-optimized second-order Møller−Plesset perturbation (OO-MP2) method to calculate HFCCs for 3d transition-metal complexes, which are difficult using the DFT method. Filatov and co-workers[27−29] have reported calculations of HFCCs using the infinite-order regular approximation (IORA) and normalized elimination of the small component (NESC) formalism in connection with high-level correlation methods, such as quadratic configuration interaction singles and doubles (QCISD) and CCSD.

Relativistic DFT methods have been widely used, because of their low computational requirements,[17−22,24,25,28] while there have been only a few studies based on *ab initio* wave function methods for relativistic HFCC calculations.[16,26,27,29] From a theoretical point of view, it is highly desirable to develop a scheme that accounts for both high-level electron correlation and relativistic effects to compute molecular HFCCs. We have previously demonstrated that the nonrelativistic density matrix renormalization group (DMRG) method,[30−41] in combination with the complete active space (CAS) model, which corresponds to the CAS configuration interaction (CASCI) and CAS self-consistent field (CASSCF) levels of theory,[39,42,43] is a promising tool for reliable predictions of isotropic HFCCs for light radicals.[44] Therefore, it is straightforward to expect that the incorporation of relativistic treatments into DMRG should be capable of accurately providing isotropic HFCCs of heavy radicals. The 4c-DMRG has been recently developed by Knecht and co-workers.[45] However, the method is still far from being ready for use in practical applications, especially for isotropic HFCCs that require the consideration of core correlation with extensive active space. Therefore, the 2c approaches are still useful for providing a good balance between computational cost and accuracy for isotropic HFCC calculations. Reiher et al. presented the incorporation of scalar relativistic effects into DMRG calculations of the potential energies of cesium hydride using the generalized arbitrary-order DKH protocol up to tenth order.[46] As a continuation of our previous work,[44] this study presents a relativistic extension of DMRG-CASSCF to evaluate the HFCCs of molecules containing heavy elements in the DKH framework.

The quasi-relativistic DKH transformation can decouple the large and small components of the Dirac spinors in the presence of an external potential by repeating unitary transformations. The main advantage of the DKH transformation is the variational stability of the DKH Hamiltonian. In addition, the DKH transformation can be easily incorporated into any electron correlation method. Numerous methods for higher-order unitary transformations have been developed, such as the exponential-type transformation,[47] the generalized transformation,[48] the infinite-order transformation,[49] and the arbitrary-order transformation.[50−52] Therefore, the DKH method has become one of the most successful approaches in relativistic quantum chemistry. Along with the success of the DKH transformation for energy-related calculations, this method has also been widely applied to the calculation of molecular properties, nuclear magnetic resonance (NMR) such as magnetic shielding constants,[53−55] NMR spin−spin coupling constants,[56] Mössbauer electron density,[57,58] electric field gradients,[59,60] magnetizabilities,[61] and HFCCs.[24−26] These studies have shown that the so-called "picture change" error (PCE) has a pronounced effect on molecular properties, even for light molecules. While the PCE correction for the higher-order DKH transformations has been implemented for the physical operators of electric field gradients, Mössbauer electron density, and magnetic shielding constants, the largest order of the DKH treatment developed for HFCCs so far is second order. Moreover, Seino et al.[62] have shown that the higher-order corrections beyond the second order are necessary to calculate with reliable accuracy the expectation value of the $\delta(r - R)$ operator, which is related to the isotropic HFCC. A similar conclusion was also recently made by Malkin et al.[17] Thus, it is necessary to extend the treatment beyond the second order to provide calculated HFCC values close to those of 4c calculations and of experiments. In the present work, we have employed the DKH transformation up to the third order (DKH3) for the hyperfine coupling (hfc) operator.

The object of this study entails two new technical points: (i) the initial derivation and implementation of the DKH3 transformation for the hfc operator, and (ii) the assessment of the performance of the DMRG in combination with the DKH transformation for isotropic HFCC calculations.

For test cases, we have applied our DMRG-CASSCF/DKH3 method to characterize the HFCCs of doublet radicals containing 4d transition metals: Ag, PdH, and $RhH_2$. Because the spin density around the vicinity of Ag nucleus is dominated by the outermost 5s orbital, the evaluation of the isotropic HFCC of atomic Ag does not require much effort. Recently, several studies using *ab initio* methods, such as QCISD/IORAmm, MP2/IORAmm,[27] and MCDF[16] have accurately predicted the isotropic HFCC of Ag. Therefore, in order to validate our derivation and implementation, we have first evaluated the isotropic HFCC of atomic Ag using different levels of DKH transformation and various sizes of active space. Pd and Rh are important in catalysis and studies on electronic and magnetic properties of their small complexes like PdH and $RhH_2$ are mostly of academic interest. In these radicals, the unpaired electron is located in the $\sigma$ orbitals that contain a predominant $4d_\sigma$ and 5s metal character and a small amount of H 1s. The reliable accuracy in characterizing the isotropic HFCC for these metal centers is thus expected to require high-order correlation and core-level spin-polarization effects. Although the EPR *g*-tensors have been calculated by numerous works using DFT and *ab initio* methods, the calculated HFCCs for the PdH radical have only been published by Belanzoni and co-workers[19] using DFT/ZORA and by Quiney and Belanzoni[15] using DHF. The isotropic HFCC of the Pd center was largely underestimated by DHF. A more reasonable result can be provided by DFT/ZORA, although the discrepancy from the experimental value is still large. Quiney and Belanzoni have attributed the failure of DHF to strong configuration mixing of the Pd orbitals, which is incapable of being described by single-configuration models like the HF theory.[15] Thus, it is interesting to assess our DMRG-CASSCF/DKH3 scheme to characterize the isotropic HFCC of the Pd center in the PdH radical. To best of our knowledge, no calculations of the EPR

parameters for the $RhH_2$ radical have yet been reported. Moreover, the experimental values are still controversial. Zee et al.[63] have measured the EPR parameters of $RhH_2$. In their experiment, the Rh atom was vaporized by laser radiation and then the vapor was deposited in an argon matrix containing hydrogen. However, the $x$-component of the hfc tensor of the Rh center measured by Zee et al. is quite uncertain [280(±60) MHz],[63] leading to unreliable HFCCs. Recently, Hayton and colleagues[64] have attempted to measure the EPR parameters of $RhH_2$ by depositing Rh atoms from thermal sources into hydrocarbon matrices. Although their results were close to those of Zee et al., they suggested that the observed spectrum should be assigned to Rh atoms instead of $RhH_2$ complexes. They also suggested that the EPR parameters measured by Zee et al. may not result from the reactions of ground-state atoms but from those of thermally and/or electronically excited Rh atoms formed in the laser plume. Another important point is that the HFCCs were obtained in matrix isolation experiments, which are assumed to involve an error of 6%−10%, relative to the gas-phase values, as pointed out by Filatov et al.[27,29] Therefore, it is important to present theoretical values using high-level theory, which correspond to the gas-phase values.

The paper is organized as follows. The background of the theory used in this study is presented in Section 2, followed by the computational details in Section 3. Results and discussion are given in Section 4. Conclusions are drawn in Section 5.

## 2. THEORETICAL BACKGROUND

**2.1. Direct DKH Transformation for the General Property Operator.** We first introduce the direct scheme of the DKH transformation for the general property operator proposed by Wolf and Reiher.[65] The general electromagnetic 4c operator $X$ can be written as follows

$$X^{(4)} = X_e^{(4)} + X_o^{(4)} \tag{1}$$

The superscript (4) indicates that the operators are in the 4c picture. The operator $X_e^{(4)}$ is even, i.e., it is a block-diagonal operator, while the operator $X_o^{(4)}$ is odd, i.e., is an off-diagonal operator. In general, the operators $X_e^{(4)}$ and $X_o^{(4)}$ are the electric and magnetic property operators, respectively. In the direct scheme, the unitary transformation $U$ only depends on an external potential $V$ and not on the property operator $X$, i.e., $U = U(V)$. The DKH property operator is then obtained by directly applying the unitary transformation $U$ to the property operator $X^{(4)}$,

$$X_{DKH\infty}^{(4)} = UX^{(4)}U^+ = \cdots U_2U_1U_0X^{(4)}U_0^+U_1^+U_2^+\cdots \tag{2}$$

with the free-particle Foldy−Wouthuysen (fpFW) transformation defined as

$$U_0 = \begin{pmatrix} A_p & A_pR_p \\ -A_pR_p & A_p \end{pmatrix} \tag{3}$$

with the operators $A_p$ and $R_p$ being given by

$$A_p = \sqrt{\frac{E_p + mc^2}{2E_p}} \tag{4}$$

$$R_p = \frac{c\boldsymbol{\sigma}\cdot\mathbf{p}}{E_p + mc^2} = K_p\boldsymbol{\sigma}\cdot\mathbf{p} \tag{5}$$

$$E_p = c\sqrt{p^2 + m^2c^2} \tag{6}$$

where $\boldsymbol{\sigma}$ denotes a 3-vector, whose elements consist of the standard $(2 \times 2)$ Pauli matrices. Wolf and Reiher[65] have argued that, to determine the DKH property operator up to $n$th order in $V$, all unitary transformations up to $U_n$ must be applied. In other words, the DKH transformation of the property operator follows the $n$ rule instead of the familiar $(2n + 1)$ rule. However, to be consistent with previous works,[24−26] the DKH order for the property operator has been defined to be the same as that for the Hamiltonian in the present work. This definition has been recently used by Seino et al.[55,62] The DKH operator $X^{(4)}$ up to third order (DKH3) then reads

$$X_{DKH3}^{(4)} = U_2U_1U_0X^{(4)}U_0^+U_1^+U_2^+ \tag{7}$$

In the present work, we employed an exponential parametrization of the unitary transformation $U_n = \exp(W_n)$, proposed by Nakajima and Hirao,[47] for $U_1$ and $U_2$. After performing the derivation, the diagonal blocks of the DKH property operators, which are exactly the same as those obtained by Wolf and Reiher,[65] read

$$X_{e,1}^{(4)} = A_p(X_e^{(4)} + R_pX_e^{(4)}R_p)A_p + \boldsymbol{\beta}A_p\{R_p, X_o^{(4)}\}A_p \tag{8}$$

$$X_{e,2}^{(4)} = X_{e,1}^{(4)} + [W_1, X_{o,1}^{(4)}] \tag{9}$$

$$X_{e,3}^{(4)} = X_{e,2}^{(4)} + \frac{1}{2}[W_1, [W_1, X_{e,1}^{(4)}]] + [W_2, X_{o,1}^{(4)}] \tag{10}$$

with the first-order off-diagonal block

$$X_{o,1}^{(4)} = \boldsymbol{\beta}A_p[R_p, X_e^{(4)}]A_p + A_p(X_o^{(4)} - R_pX_o^{(4)}R_p)A_p \tag{11}$$

The odd operators $W_1$ and $W_2$ are the familiar perturbation-independent operators parametrizing the standard unitary transformation $U_1$ and $U_2$, respectively:

$$W_1(p, p') = \boldsymbol{\beta}\frac{O_1(p, p')}{E_{p'} + E_p} \tag{12}$$

$$W_2(p, p') = \boldsymbol{\beta}\frac{[W_1(p, p'), E_1(p, p')]}{E_{p'} + E_p} \tag{13}$$

The operators $E_1$ and $O_1$ are given by the expressions

$$E_1 = A_pVA_p + A_pR_pVR_pA_p \tag{14}$$

$$O_1 = A_pR_pVA_p + A_pVR_pA_p \tag{15}$$

**2.2. Direct DKH Transformation for Magnetic Operator.** The 4c magnetic operator describing the interaction between the electron spin and a magnetic field is given by

$$X = \begin{pmatrix} 0 & \boldsymbol{\sigma}\cdot\mathbf{A} \\ \boldsymbol{\sigma}\cdot\mathbf{A} & 0 \end{pmatrix} \tag{16}$$

where $\mathbf{A}$ refers to the vector potential of the magnetic field. We substitute the 4c operator described in eq 16 into eqs 8−11. Because the magnetic operator described in eq 16 is odd, only terms related to $X_o^{(4)}$ are nonzero. After performing the derivation, we finally obtain the upper diagonal block of DKH3 magnetic operator as follows:

$$X_{e,1}^{(2)} = H_{mag} + H_{mag}^+ \tag{17}$$


dx.doi.org/10.1021/ct5007778 | J. Chem. Theory Comput. XXXX, XXX, XXX−XXX

$$X^{(2)}_{e,2} = X_{e,1} - (A\tilde{V}A)H_{mag} + (AR\tilde{V}RA)R_p^{-2}H_{mag} - (AR\tilde{V}RA)H^+_{mag} + (A\tilde{V}A)R_p^2H^+_{mag} - H^+_{mag}(A\tilde{V}A) + H^+_{mag}R_p^{-2}(AR\tilde{V}RA) - H_{mag}(AR\tilde{V}RA) + H_{mag}R_p^2(A\tilde{V}A) \quad (18)$$

$$\begin{aligned} X^{(2)}_{e,3} = {} & X_{e,2} + (AR\tilde{V}RA)H^+_{mag}(A\tilde{V}A) + (A\tilde{V}A)H_{mag}(AR\tilde{V}RA) \\ & + (A\tilde{V}A)R_p^2H^+_{mag}R_p^{-2}(AR\tilde{V}RA) + (AR\tilde{V}RA)R_p^{-2}H_{mag}R_p^2(A\tilde{V}A) \\ & - (A\tilde{V}A)R_p^2H^+_{mag}(A\tilde{V}A) - (A\tilde{V}A)H_{mag}R_p^2(A\tilde{V}A) \\ & - (AR\tilde{V}RA)H^+_{mag}R_p^{-2}(AR\tilde{V}RA) - (AR\tilde{V}RA)R_p^{-2}H_{mag}(AR\tilde{V}RA) \\ & + (AR\tilde{V}RA)R_p^{-2}(AR\tilde{V}RA)R_p^{-2}H_{mag} \\ & - (AR\tilde{V}RA)R_p^{-2}(AR\tilde{V}RA)H^+_{mag} + (AR\tilde{V}RA)(A\tilde{V}A)H_{mag} \\ & - (AR\tilde{V}RA)(A\tilde{V}A)R_p^2H^+_{mag} - (A\tilde{V}A)(AR\tilde{V}RA)R_p^{-2}H_{mag} \\ & + (A\tilde{V}A)(AR\tilde{V}RA)H^+_{mag} + (A\tilde{V}A)R_p^2(A\tilde{V}A)H_{mag} \\ & + (A\tilde{V}A)R_p^2(A\tilde{V}A)R_p^2H^+_{mag} - H^+_{mag}R_p^{-2}(AR\tilde{V}RA)(A\tilde{V}A) \\ & + H^+_{mag}R_p^{-2}(AR\tilde{V}RA)R_p^{-2}(AR\tilde{V}RA) - H^+_{mag}(A\tilde{V}A)R_p^2(A\tilde{V}A) \\ & + H^+_{mag}(A\tilde{V}A)(AR\tilde{V}RA) + H_{mag}(AR\tilde{V}RA)(A\tilde{V}A) \\ & - H_{mag}(AR\tilde{V}RA)R_p^{-2}(AR\tilde{V}RA) + H_{mag}R_p^2(A\tilde{V}A)R_p^2(A\tilde{V}A) \\ & - H_{mag}R_p^2(A\tilde{V}A)(AR\tilde{V}RA) - (A\tilde{V}A)(AR\tilde{V}RA)R_p^{-2}H_{mag} \\ & + (A\tilde{V}A)(AR\tilde{V}RA)H^+_{mag} + (A\tilde{V}A)(A\tilde{V}A)H_{mag} \\ & - (A\tilde{V}A)(A\tilde{V}A)R_p^2H^+_{mag} - (AR\tilde{V}RA)(AR\tilde{V}RA)R_p^{-2}H_{mag} \\ & + (AR\tilde{V}RA)(AR\tilde{V}RA)H^+_{mag} + (AR\tilde{V}RA)(A\tilde{V}A)H_{mag} \\ & - (AR\tilde{V}RA)(A\tilde{V}A)R_p^2H^+_{mag} + H^+_{mag}(A\tilde{V}A)(A\tilde{V}A) \\ & + H^+_{mag}(A\tilde{V}A)(AR\tilde{V}RA) - H^+_{mag}R_p^{-2}(AR\tilde{V}RA)(A\tilde{V}A) \\ & - H^+_{mag}R_p^{-2}(AR\tilde{V}RA)(AR\tilde{V}RA) - H_{mag}R_p^2(A\tilde{V}A)(A\tilde{V}A) \\ & - H_{mag}R_p^2(A\tilde{V}A)(AR\tilde{V}RA) + H_{mag}(AR\tilde{V}RA)(A\tilde{V}A) \\ & + H_{mag}(AR\tilde{V}RA)(AR\tilde{V}RA) \end{aligned} \quad (19)$$

where

$$A\tilde{V}A = A_p\left(\frac{V(p,p')}{E_p + E_{p'}}\right)A_p \quad (20)$$

$$AR\tilde{V}RA = A_pR_p\left(\frac{V(p,p')}{E_p + E_{p'}}\right)R_pA_p \quad (21)$$

and

$$H_{mag} = A_pK_p(\boldsymbol{\sigma}\cdot\mathbf{p})(\boldsymbol{\sigma}\cdot\mathbf{A})A_p \quad (22)$$

$$H^+_{mag} = A_p(\boldsymbol{\sigma}\cdot\mathbf{A})(\boldsymbol{\sigma}\cdot\mathbf{p})K_pA_p \quad (23)$$

The superscript (2) in eqs 17−19 means that the DKH operators are in the 2c picture.

Using the relation

$$(\boldsymbol{\sigma}\cdot\mathbf{a})(\boldsymbol{\sigma}\cdot\mathbf{b}) = \mathbf{a}\cdot\mathbf{b} + i\boldsymbol{\sigma}\cdot(\mathbf{a}\times\mathbf{b}) \quad (24)$$

we have

$$\begin{aligned} (\boldsymbol{\sigma}\cdot\mathbf{p})(\boldsymbol{\sigma}\cdot\mathbf{A}) &= \mathbf{p}\cdot\mathbf{A} + i\boldsymbol{\sigma}\cdot(\mathbf{p}\times\mathbf{A}) \\ &= [\mathbf{p}\cdot\mathbf{A}] + \mathbf{A}\cdot\mathbf{p} + i\boldsymbol{\sigma}\cdot[\mathbf{p}\times\mathbf{A}] - i\boldsymbol{\sigma}\cdot(\mathbf{A}\times\mathbf{p}) \end{aligned} \quad (25)$$

$$(\boldsymbol{\sigma}\cdot\mathbf{A})(\boldsymbol{\sigma}\cdot\mathbf{p}) = \mathbf{A}\cdot\mathbf{p} + i\boldsymbol{\sigma}\cdot(\mathbf{A}\times\mathbf{p}) \quad (26)$$

Here, the square brackets mean that the operator $\mathbf{p}$ only acts on the vector potential $\mathbf{A}$ and not on the wave function. It is easy to show that the first term in eq 25 vanishes. In fact, this term will vanish if we invoke the Coulomb gauge $\nabla\cdot\mathbf{A} = 0$.[66] From eqs 25 and 26, it is easy to decompose the magnetic operator into various contributions. The linear terms in $\sigma$ represent the spin contribution, while the other terms represent the orbital contribution.

Substituting eqs 22 and 23 into eqs 17−19 and using the relations described by eqs 25 and 26, we obtain the DKH transformation for the magnetic operator. For example, the first order of the DKH magnetic operator reads

$$X^{(2)}_{e,1} = A_pK_pi\boldsymbol{\sigma}\cdot[\mathbf{p}\times\mathbf{A}]A_p - A_pi\boldsymbol{\sigma}\cdot\{K_p(\mathbf{A}\times\mathbf{p}) - (\mathbf{A}\times\mathbf{p})K_p\}A_p + A_p\{K_p\mathbf{A}\cdot\mathbf{p} + \mathbf{A}\cdot\mathbf{p}K_p\}A_p \quad (27)$$

Neyman et al.[67] neglected the second term in eq 27 in their implementation, and Malkin et al.[68] have subsequently confirmed that the contribution of this term is completely negligible. In the NR limit ($c \to \infty$), the kinetic factors $A_p \to 1$ and $K_p \to (2c)^{-1}$. The NR operator can be then obtained.

It is worth mentioning that, although the third-order expression is relatively long, its computational cost is comparable to that of the second-order expression.

**2.3. Hyperfine Coupling Operator.** In the case of the hfc operator, the vector potential created by nucleus $N$ is given as follows:

$$\mathbf{A}_N = \boldsymbol{\mu}_N \times \nabla G_N \quad (28)$$

where $\boldsymbol{\mu}_N$ is the magnetic moment of nucleus $N$ and

$$G_N = \int \frac{\chi_N(\mathbf{R} - \mathbf{R}_N)}{\mathbf{r} - \mathbf{R}_N}\,\mathrm{d}\mathbf{R} \quad (29)$$

Here, $\mathbf{r}$ and $\mathbf{R}$ are the electronic and nuclear distributions, respectively, and $\chi_N$ is the function related to the nuclear magnetization distribution, which is usually assumed to be the same as the nuclear charge distribution in quantum chemical calculations.[26,69] Here, we use the Gaussian nucleus model

$$\chi(\mathbf{R} - \mathbf{R}_N) = \left(\frac{\eta_N}{\pi}\right)^{3/2}\exp(-\eta_N(\mathbf{R} - \mathbf{R}_N)^2) \quad (30)$$

The nuclear exponent $\eta_N$ is taken from the database reported by Visscher and Dyall.[70]

An additional integral $[\mathbf{A}\times\mathbf{p}]$, which is related to the second term in eq 27, was implemented. We numerically found that the total contribution of the terms related to this integral is negligible not only at the first order, but at higher orders. This confirms the earlier work of Malkin et al.[68] Thus, we will not discuss it hereafter. In the present work, we only consider the SR effects, so that the orbital contribution, which is related to the inner product $[\mathbf{A}\cdot\mathbf{p}]$, is also neglected.

Using the vector potential described by eq 28, the third term of eq 25 reads[66]

$$h^{(\sigma)}_{hfc} = i\boldsymbol{\sigma}\cdot[\mathbf{p}\times\mathbf{A}_N] = h_{iso} + h_{ani} \quad (31)$$

where the first and second terms in eq 31 are the isotropic (iso) and anisotropic (ani) contributions, respectively:

$$h_{iso} = \frac{2}{3}(i\boldsymbol{\sigma}\cdot\boldsymbol{\mu}_N)(\mathbf{p}\cdot\nabla G_N) \quad (32)$$


dx.doi.org/10.1021/ct5007778 | J. Chem. Theory Comput. XXXX, XXX, XXX−XXX

$$h_{\mathrm{ani}} = -\left[(\boldsymbol{\mu}_N\cdot\mathbf{p})(i\boldsymbol{\sigma}\cdot\nabla G_N) - \frac{1}{3}(i\boldsymbol{\sigma}\cdot\boldsymbol{\mu}_N)(\mathbf{p}\cdot\nabla G_N)\right] \quad (33)$$

The HFCCs of nucleus $N$ are finally determined as follows:

$$A_{uv}(N) = \frac{\partial}{\partial S^u}\left\langle \psi \left| \frac{\partial X_{\mathrm{DKH}}(\boldsymbol{\sigma})}{\partial \mu_N^v} \right| \psi \right\rangle \quad (34)$$

where the indices $u$ and $v$ denote $x$, $y$, and $z$; $\mathbf{S}$ refers to the spin vector; and $X_{\mathrm{DKH}}(\boldsymbol{\sigma})$ is the DKH spin-dependent hfc operator.

## 3. COMPUTATIONAL DETAILS

We used a DMRG code developed by our group[41] to obtain the active-space wave function. The active spaces used in this work are presented in Table 1. The number of spin-adapted renormalized states $M$ was set to 512 in all DMRG calculations, unless otherwise noted. We have implemented the spin adaptation of Zgid and Nooijen[38] in our DMRG code; therefore, the number of actual bases that are not spin-adapted is much larger than $M$ (approximately twice). According to the assessment of the convergence of HFCCs with respect to $M$ in our previous work,[44] DMRG calculations with $M$ = 512 can provide reliable HFCCs. The macro-iteration threshold of the DMRG-CASSCF calculations is $1.00 \times 10^{-3}$, except for the largest CAS in the cases of PdH and $RhH_2$ (see Table 1), where it is $2.00 \times 10^{-3}$. Below these thresholds, the calculated HFCC values are found to converge with a numerical fluctuation of <1%. The uncontracted ANO basis sets[71,72] were used for all elements and have the following numbers of exponents: 21s 18p 13d 6f for metals (Ag, Pd, and Rh) and 8s 4p 3d for H.

**Table 1. Active Orbitals**

| molecule | active space | active orbitals | |
|---|---|---|---|
| Ag | CAS(19e,18o) | 4s 4p 4d 5s 5p 5d | |
| | CAS(37e,32o) | 3s 3p 3d 4s 4p 4d 5s 5p 5d 6d | |
| | CAS(37e,39o) | 3s 3p 3d 4s 4p 4d 5s 5p 5d 6d 4f | |
| PdH | CAS(21e,20o) | Pd: 3s 4s 4p 4d 5s 5p 5d | H: 1s |
| | CAS(21e,32o) | Pd: 3s 4s 4p 4d 5s 5p 5d 6d 4f | H: 1s |
| | CAS(37e,40o) | Pd: 3s 3p 3d 4s 4p 4d 5s 5p 5d 6d 4f | H: 1s |
| $RhH_2$ | CAS(21e,21o) | Rh: 3s 4s 4p 4d 5s 5p 5d | H: 1s |
| | CAS(21e,33o) | Rh: 3s 4s 4p 4d 5s 5p 5d 6d 4f | H: 1s |
| | CAS(37e,41o) | Rh: 3s 3p 3d 4s 4p 4d 5s 5p 5d 6d 4f | H: 1s |

The molecular geometry of PdH was taken from experiment: Pd−H = 1.529 Å.[19] Because there is no available experimental geometry for the $RhH_2$ radical, we have adapted it from the MRCI-SD calculation reported by Balasubramanian and Liao:[73] Rh−H = 1.510 Å and ∠H−Rh−H = 84° for the ground-state $^2A_1$.

For comparison, the scalar relativistic calculations based on ZORA Hamiltonian were performed to evaluate HFCCs using the DFT method with three functionals: the hybrid-GGA functional B3LYP,[8,9] pure-GGA functional BP86,[74,75] and the Hartree−Fock (HF) method. The program suite NWCHEM[76] was employed to carry out B3LYP/ZORA, BP86/ZORA, and HF/ZORA calculations with and without the paramagnetic-spin−orbit (PSO) correction, which is evaluated using the linear response (or coupled-perturbed) theory in the framework of the second-order treatment. Note (naïvely) that we additionally attempted to use the program ORCA[77] for DFT/ZORA calculations; however, it was found, in some cases, to provide results that were inconsistent with those obtained with NWCHEM at the same level of theory; this may arise from numerical sensitivity associated with our uncontracted basis sets.

In the present work, the orders of the DKH transformation are common for the DKH Hamiltonian and PCE-corrected hfc operator and, therefore, a nonredundant notation DKH$n$ was used instead of DKH$n$−DKH$n$, where the first is for the Hamiltonian and the second is for the hfc operator. The FN model described by a Gaussian distribution (eq 30) was used for all DMRG calculations, while the point charge (PC) nuclear model was used for our DFT/ZORA calculations.

The most computationally intensive part of the HFCC calculations using our code is the step to diagonalize active space Hamiltonian with DMRG algorithm. This step is repeated several times for orbital optimization, a procedure of CASSCF algorithm.[42] The computational times of a single step of the DMRG calculations with M = 512 carried out on the single Intel-based Linux node with 12 CPU cores were ∼2 h and 2 days for CAS(21e,20o) and CAS(21,32o), respectively, in the case of PdH, and ∼6 h and 2 days for CAS(21e,21o) and CAS(21,33o), respectively, in the case of $RdH_2$.

## 4. RESULTS AND DISCUSSION

**4.1. Silver (Ag) Atom.** We evaluated the isotropic HFCC of the Ag atom in order to assess our derivation and implementation. The isotropic HFCC, as functions of DKH order and active space, is presented in Figure 1. The experimental value (−1717 MHz) was taken from ref 78.

We now consider the correlation effects. Because the convergence behavior of the isotropic HFCC with respect to the active space is similar at different DKH orders, we only discuss the results at the DKH3 level. The isotropic HFCC clearly converges smoothly with increasing size of the active space. The DMRG-CASSCF(19e,18o) value greatly underestimates the isotropic HFCC. With the active space extended to CAS(37e,32o), including extra core orbitals and one 6d shell, the calculated HFCC value increases reasonably, comparable with the experimental value. By further extending the active space with the inclusion of the polarization 4$f$ shell, the isotropic HFCC slightly increases and is in excellent agreement with the experimental value.

We next discuss the relativistic effects. The lower panel of Figure 1 presents the percentage errors of the calculated results relative to the experimental value at different DKH orders using the DMRG-CASSCF(37e,39o) calculation. Although the DKH1 level improves the isotropic HFCC over the NR level, its result is still far from the experimental value. This means that the transformation of the Hamiltonian, as well as the magnetic operator, at the DKH1 level is insufficient to obtain an accurate result. Our observation is consistent with many previous works.[53−56,58,62] When the DKH level goes from first order to second order, the error significantly decreases from 30% to 4%. Finally, the correction to the third-order expression improves the result further, such that it quite closely agrees with the experimental value.

Here, let us briefly mention the convergence of isotropic HFCC values with respect to the quality of basis set. We tested an extended basis set that was derived by adding four $g$ functions to the basis set used in the above benchmark calculations. Because the DMRG-CASSCF calculations with large active space were too demanding in conjunction with large basis set, we employed the reduced active space

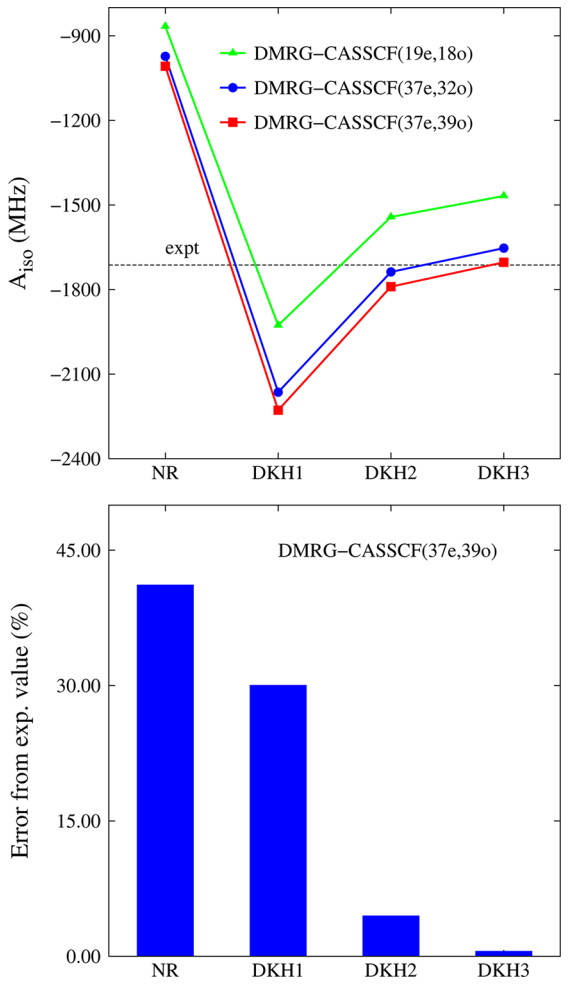


**Figure 1.** (Upper panel) Isotropic HFCC of Ag atom with different levels of DKH transformation and various sizes of active space. (Lower panel) Percentage errors of the DMRG-CASSCF(37e,39o) results, relative to the experimental value, as a function of the DKH order.

CAS(19e,18o). The result obtained with the given basis set (−1467.99 MHz) was more or less the same as that with the extended basis set (−1468.09 MHz). Therefore, it seems that the given uncontracted basis set (Table 1) is sufficient for isotropic HFCC calculation.

This assessment of the performance of the DMRG-CASSCF/DKH method with different levels of DKH order and various sizes of active space for predicting the isotropic HFCC for Ag atom shows that the error in the DMRG-CASSCF(37e,39o)/DKH3 result, relative to the experimental value, can be decreased to <1%.

**4.2. PdH Radical.** We now consider the PdH radical. All the theoretical results calculated for the PdH radical in this work are summarized in Table 2, along with the experimental values in the Ar and Ne matrices.[78] For comparison, the results reported by Belanzoni and co-workers[15,19] are also presented. In the experiment and the works of Belanzori et al., the parallel component ($A_{\parallel}$) and the perpendicular component ($A_{\perp}$) were provided and, therefore, in order to extract the $A_{iso}$ and $A_{ani}$ values from $A_{\parallel}$ and $A_{\perp}$, we used the following formulas:

$$A_{iso} = \frac{A_{\parallel} + 2A_{\perp}}{3} \tag{35}$$

**Table 2. HFCCs of the Pd Center in the PdH Radical[a]**

| | HFCC (MHz) | |
|---|---|---|
| method | $A_{iso}$(Pd) | $A_{ani}$(Pd) |
| BP86/ZORA[b] | −910 | 29 |
| DHF[c] | 552 | −7 |
| B3LYP/ZORA | | |
| uncorrected | −820.87 | 34.20 |
| PSO-corrected | −862.24 | 14.65 |
| BP86/ZORA | | |
| uncorrected | −925.15 | 29.25 |
| PSO-corrected | −958.82 | 13.05 |
| UHF/ZORA | | |
| uncorrected | −437.90 | 51.24 |
| PSO-corrected | −514.09 | 16.16 |
| UHF/DKH2 | −523.13 | 52.23 |
| UHF/DKH3 | −498.77 | 52.21 |
| DMRG-CASSCF(21e,20o)/DKH2 | −878.57 | 39.50 |
| DMRG-CASSCF(21e,32o)/DKH2 | −939.23 | 45.88 |
| DMRG-CASSCF(37e,40o)/DKH2 | −913.90 | 38.65 |
| DMRG-CASSCF(21e,20o)/DKH3 | −842.02 | 40.82 |
| DMRG-CASSCF(21e,32o)/DKH3 | −895.35 | 45.89 |
| DMRG-CASSCF(37e,40o)/DKH3 | −872.00 | 38.54 |
| experiment | | |
| Ne-matrix[d] | −857 (±4) | 16 |
| Ar-matrix[d] | −823 (±4) | 22 |

[a]All DMRG calculations were performed using $M$ = 512. [b]Data taken from ref 19. [c]Data taken from ref 15. [d]Data taken from ref 79.

$$A_{ani} = \frac{A_{\parallel} - A_{\perp}}{3} \tag{36}$$

We mainly focus on the isotropic HFCC of the Pd center. According to the results reported by Belanzoni and co-workers, the DHF severely underestimates the isotropic HFCC of the Pd center, while a reasonable result can be obtained using BP86/ZORA. The present DFT/ZORA calculations overall yielded the HFCCs of the Pd center with the accuracy comparable to the previous BP86/ZORA results. With the paramagnetic spin−orbit (PSO) correction, $A_{iso}$ was slightly enhanced by a factor of ∼5%, while a pronounced effect was observed on $A_{ani}$ and the resulting anisotropic contribution became much closer to the Ne-matrix value than that without the PSO correction. The unrestricted Hartree−Fock (UHF) results underestimated the isotropic HFCC of the Pd center by approximately one-half, relative to the Ne-matrix value, highlighting that correlation effects play a significant role. We here note that DFT/ZORA calculations neglected the FN effect; however, the previous studies[25,80] showed that the FN effect reduces the isotropic HFCC of Ag atom by 3%−15%. Comparison of the UHF results between the ZORA and DKH3 relativistic treatments (437.90 and 498.77 MHz, respectively) indicates that ZORA relatively underestimates the absolute value of isotropic HFCC.

For the DMRG-CASSCF/DKH2 calculations, the result for CAS(21e,20o) is in good agreement with the Ne-matrix value, with a relative error of 3%. However, when the active space is enlarged to CAS(21e,32o), the isotropic HFCC of the Pd center increases. According to Filatov et al.,[27,29] the increase of the isotropic HFCC is due to contraction of the atomic inner shell electrons toward the nucleus under the effect of electron correlation. With further increases in the active space to CAS(37e,40o), the isotropic HFCC of the Pd center decreases


dx.doi.org/10.1021/ct5007778 | J. Chem. Theory Comput. XXXX, XXX, XXX−XXX

and the relative error is 7%. This means that the DMRG-CASSCF(37e,40o) has captured the higher-order correlation, which is required for realistic accuracy of the isotropic HFCC of the Pd center, as expected. The third-order correction of the DKH treatment reduces the absolute values of the isotropic HFCCs obtained from the DMRG-CASSCF/DKH2 calculations, leading to a better agreement with the experimental value. The variation of the isotropic HFCCs with the size of the active space in the case of the third order is similar to that in the case of the second order. The error in the DMRG-CASSCF(37e,40o)/DKH3 result, relative to the Ne-matrix value, is observed to be 2%.

The anisotropic HFCCs are less sensitive to the DKH order. Similar to the isotropic HFCC, the variation of the anisotropic HFCC, with respect to the active space, is nonmonotonic.

**4.3. $RhH_2$ Radical.** All the theoretical and experimental values for the $RhH_2$ radical are collected in Table 3. In the experiments, only the absolute values of the isotropic HFCC were reported and, hence, for consistency, we also present the absolute values of calculated isotropic HFCCs, which were, in fact, obtained to be negative. Because the DMRG-CASSCF-(37e,41o) calculation with $M$ = 512 is computationally demanding, the results for DMRG-CASCI(37e,41o) with $M$ = 512 were obtained using the converged orbitals from DMRG-CASSCF(37e,41o) with $M$ = 256. According to the DMRG-CASSCF(37e,40o) calculation for PdH in the previous subsection, the deviation of the result with $M$ = 256 from that with $M$ = 512 is ∼2%. Thus, we believe that all results for DMRG-CASSCF with M = 256 in this work are reliable. It would be valuable to provide further results at the HF level, namely, UHF and restricted open-shell Hartree−Fock (ROHF).

**Table 3. HFCCs of the Rh Center in the $RhH_2$ Radical[a]**

| | HFCCs (MHz) | | | |
|---|---|---|---|---|
| method | $\lvert A_{iso}\rvert$ | $A^x_{ani}$ | $A^y_{ani}$ | $A^z_{ani}$ |
| B3LYP/ZORA | | | | |
| uncorrected | 251.46 | 33.17 | −17.79 | −15.38 |
| PSO-corrected | 308.35 | −22.01 | 5.52 | 16.49 |
| BP86/ZORA | | | | |
| uncorrected | 297.26 | 33.39 | −18.50 | −14.89 |
| PSO-corrected | 339.04 | −7.47 | −0.36 | 7.83 |
| UHF/ZORA | | | | |
| uncorrected | 129.62 | 21.85 | −14.54 | −7.30 |
| PSO-corrected | 205.85 | −39.81 | 9.63 | 30.18 |
| UHF/DKH2 | 155.08 | 20.72 | −14.13 | −6.60 |
| UHF/DKH3 | 148.02 | 20.73 | −14.12 | −6.61 |
| ROHF/DKH3 | 196.06 | 50.05 | −24.81 | −25.24 |
| DMRG-CASSCF(21e,21o)/DKH3 | 431.06 | 48.92 | −36.55 | −12.36 |
| DMRG-CASSCF(21e,33o)/DKH3 | 344.46 | 21.20 | −22.59 | 1.38 |
| DMRG-CASSCF(37e,41o)/DKH3[b] | 303.29 | 39.12 | −20.82 | −18.29 |
| experiment, Ar-matrix[c] | 268(±20) | 12 | −20 | 8 |

[a]DMRG calculations for CAS(21e,21o) and CAS(21e,33o) were performed using $M$ = 512. [b]DMRG-CASCI with $M$ = 512, using converged orbitals from DMRG-CASSCF with $M$ = 256. [c]Data taken from ref 63.

We now discuss the isotropic HFCC of the Rh center. The isotropic HFCC was obtained with the UHF method at three different levels of relativistic treatment—DKH2, DKH3, and ZORA—so that we can examine the impact of level at which the relativistic operator is evaluated. As discussed earlier, the ZORA values are underestimated in magnitude compared to the DKH3 values; the error of UHF/ZORA relative to UHF/DK3 was observed to be ∼12%. A similar magnitude of error seems to be involved in DFT/ZORA results.

For the DMRG/DKH3 calculations, the isotropic HFCC of the Rh center converges smoothly, with respect to the size of the active space. The result of CAS(21e,21o) is much higher than the experimental value with an error relative to the average experimental value of 61%. The inclusion of the 6d and 4f shells in the active space, i.e., CAS(21e,33o), leads to a significant reduction in the relative error (from 61% to 28%). From the results of these two active spaces, it is found that including only the inner shell 3s is not sufficient to obtain a result comparable to the experimental value. Enlarging the active space to CAS(37e,41o), i.e., including the 3p 3d orbitals (see Table 1), significantly decreases the error, relative to the average experimental value to ∼13%, close to the upper limit (error of ∼5%). When the FN effect is taken into account, the isotropic HFCC is nonlocal, and is dependent not only on the spin density at the nucleus position, but also on the spin density in the vicinity of the nucleus. Thus, including the 3p 3d inner shells might lead to a proper description of the spin density in the vicinity of the Rh center. The error of the isotropic HFCCs obtained with DMRG-CASSCF(37e,41o), relative to the experiment, may be explained as follows:

(i) In the experiment, the $x$-component of the hfc tensor suffered a large error bar [$A_x$ = 280 (±60) MHz].[63]
(ii) The calculated HFCCs correspond to the gas-phase values, whereas the experimental measurement was performed in the Ar matrix isolation.
(iii) The geometry used in this study is not from the experiment, but from MRCI-SD calculation.[73]
(iv) Another posibility is that the DMRG-CASSCF results may not be fully converged, with respect to the size of the active space.

The B3LYP/ZORA and BP86/ZORA results without PSO correlation are in reasonably good agreement with the DMRG-CASSCF results with the largest CAS reference. The absolute value of $A_{iso}$ obtained with BP86/ZORA is overestimated, compared to that with B3LYP/ZORA (with an error of 18%), as also observed for PdH. The calculations at the HF/DKH3 level also significantly underestimate the isotropic HFCC of the Rh center; the relative errors of the results from the HF/DKH3 calculations are 45% and 27% for UHF and ROHF, respectively.

We now briefly discuss the anisotropic HFCC of the Rh center. The experimental anisotropic HFCCs were extracted using the formula

$$A^i_{ani} = |A_i| - |A_{iso}|$$

where $i$ = $x$, $y$, $z$. According to the work of Zee et al.,[63] the experimental anisotropic HFCCs are meaningless, because of the uncertainty in the $x$-component. If the upper limit of $A_x$ is used (i.e., 340 MHz), $A^x_{ani}$, $A^y_{ani}$, and $A^z_{ani}$ would be 52 MHz, −40 MHz, and −12 MHz, respectively, which turn out to be roughly in good agreement with the anisotropic HFCCs obtained with our DFT, UHF, and DMRG-CASSCF calculations without


dx.doi.org/10.1021/ct5007778 | J. Chem. Theory Comput. XXXX, XXX, XXX−XXX

PSO correction. The correlation effect considered by DMRG-CASSCF/DKH3 reduces the absolute value of the anisotropic HFCCs obtained from the uncorrelated ROHF/DKH3 calculation. The DMRG-CASSCF/DKH3 results are seemingly sensitive to the active space but fall in the range between the average and upper limit values.

## 5. CONCLUSION

In summary, we have developed a new computational scheme including the high-level electron correlation effects as well as the SR effects for the accurate prediction of the isotropic HFCC of heavy molecules. For electron correlation, we employed the DMRG method in the framework of the CAS model. The orbital-optimization procedure, i.e., DMRG-CASSCF, was employed to obtain the optimized orbitals required for accurate determination of the isotropic HFCC, as shown in our previous work.[44] For the SR effects, we have derived and implemented the DKH hfc operators up to third order by using the direct transformation scheme. The primitive ANO basis set and FN model were used for all DMRG calculations.

As test cases, we have evaluated the HFCCs for several 4d transition-metal radicals: Ag atom, PdH, and $RhH_2$. Good agreement between the isotropic HFCC values obtained from DMRG-CASSCF/DKH3 and experiment was found, especially for the case of Ag atom, which was obtained from the gas phase.[78] We note that the HFCCs of PdH and $RhH_2$ were measured in inert gas matrices. According to Filatov et al.,[27,29] the effect of the inert gas matrices on the experimental values may reach as much as 6%−10%. Thus, the difference between calculated and experimental isotropic HFCCs seems reasonable.

## AUTHOR INFORMATION


### Corresponding Author

*E-mail: lantrann@gmail.com.

### Present Address

[∇]Ho Chi Minh City Institute of Physics, VAST, Ho Chi Minh City, Vietnam.


### Notes

The authors declare no competing financial interest.

## ACKNOWLEDGMENTS

The authors are grateful to Dr. Jakub Chalupský for valuable discussions and careful reading of the manuscript. Y.K. and T.Y. were supported by Grant-in-Aid for Scientific Research (B) (Grant No. 25288013), and Y.K. by Grant-in-Aid for Scientific Research (C) (Grant No. 25410030) and on Innovative Areas "Soft Molecular Systems" (Grant No. 26104538), from Ministry of Education, Culture, Sports, Science and Technology-Japan (MEXT). Y.K. was supported by a grant of Morino Foundation for Molecular Science.

## REFERENCES


(1) Sekino, H.; Bartlett, R. J. *J. Chem. Phys.* **1985**, *82*, 4225−4228.
(2) Perera, S. A.; Watts, J. D.; Bartlett, R. J. *J. Chem. Phys.* **1994**, *100*, 1425−1432.
(3) Momose, T.; Nakatsuji, H.; Shida, T. *J. Chem. Phys.* **1988**, *89*, 4185−4192.
(4) Momose, T.; Yamaguchi, M.; Shida, T. *J. Chem. Phys.* **1990**, *93*, 7284−7292.
(5) Chipman, D. M. *Theor. Chim. Acta* **1992**, *82*, 93−115.
(6) Engels, B. *Chem. Phys. Lett.* **1991**, *179*, 398−404.
(7) Engels, B. *J. Chem. Phys.* **1994**, *100*, 1380−1386.
(8) Lee, C.; Yang, W.; Parr, R. G. *Phys. Rev. B* **1988**, *37*, 785−789.
(9) Becke, A. D. *J. Chem. Phys.* **1993**, *98*, 5648−5652.
(10) Perdew, J. P.; Burke, K.; Ernzerhof, M. *Phys. Rev. Lett.* **1996**, *77*, 3865−3868.
(11) Perdew, J. P.; Burke, K.; Ernzerhof, M. *Phys. Rev. Lett.* **1997**, *78*, 1396−1396.
(12) Kossmann, S.; Kirchner, B.; Neese, F. *Mol. Phys.* **2007**, *105*, 2049−2071.
(13) Tao, J.; Perdew, J. P.; Staroverov, V. N.; Scuseria, G. E. *Phys. Rev. Lett.* **2003**, *91*, No. 146401.
(14) Grimme, S. *J. Chem. Phys.* **2006**, *124*, No. 034108.
(15) Quiney, H. M.; Belanzoni, P. *Chem. Phys. Lett.* **2002**, *353*, 253−258.
(16) Song, S.; Wang, G.; Ye, A.; Jiang, G. *J. Phys. B* **2007**, *40*, 475−484.
(17) Malkin, E.; Repiský, M.; Komorovský, S.; Mach, P.; Malkina, O. L.; Malkin, V. G. *J. Chem. Phys.* **2011**, *134*, No. 044111.
(18) van Lenthe, E.; van der Avoird, A.; Wormer, P. E. S. *J. Chem. Phys.* **1998**, *108*, 4783−4796.
(19) Belanzoni, P.; van Lenthe, E.; Baerends, E. J. *J. Chem. Phys.* **2001**, *114*, 4421−4433.
(20) Aquino, F.; Pritchard, B.; Autschbach, J. *J. Chem. Theory Comput.* **2012**, *8*, 598−609.
(21) Autschbach, J.; Patchkovskii, S.; Pritchard, B. *J. Chem. Theory Comput.* **2011**, *7*, 2175−2188.
(22) Verma, P.; Autschbach, J. *J. Chem. Theory Comput.* **2013**, *9*, 1932−1948.
(23) Autschbach, J. *Theor. Chem. Acc.* **2004**, *112*, 52−57.
(24) Malkin, I.; Malkina, O. L.; Malkin, V. G.; Kaupp, M. *Chem. Phys. Lett.* **2004**, *396*, 268−276.
(25) Malkin, E.; Malkin, I.; Malkina, O. L.; Malkin, V. G.; Kaupp, M. *Phys. Chem. Chem. Phys.* **2006**, *8*, 4079−4085.
(26) Sandhoefer, B.; Kossmann, S.; Neese, F. *J. Chem. Phys.* **2013**, *138*, No. 104102.
(27) Filatov, M.; Cremer, D. *J. Chem. Phys.* **2004**, *121*, 5618−5622.
(28) Filatov, M.; Cremer, D. *J. Chem. Phys.* **2005**, *123*, No. 124101.
(29) Filatov, M.; Zou, W.; Cremer, D. *J. Phys. Chem. A* **2012**, *116*, 3481−3486.
(30) White, S. R. *Phys. Rev. Lett.* **1992**, *69*, 2863−2866.
(31) White, S. R. *Phys. Rev. B* **1993**, *48*, 10345−10356.
(32) White, S. R.; Martin, R. L. *J. Chem. Phys.* **1999**, *110*, 4127−4130.
(33) Mitrushenkov, A. O.; Fano, G.; Ortolani, F.; Linguerri, R.; Palmieri, P. *J. Chem. Phys.* **2001**, *115*, 6815−6821.
(34) Chan, G. K.-L.; Head-Gordon, M. *J. Chem. Phys.* **2002**, *116*, 4462−4476.
(35) Chan, G. K.-L.; Head-Gordon, M. *J. Chem. Phys.* **2003**, *118*, 8551−8554.
(36) Legeza, Ö.; Röder, J.; Hess, B. A. *Phys. Rev. B* **2003**, *67*, No. 125114.
(37) Moritz, G.; Reiher, M. *J. Chem. Phys.* **2007**, *126*, No. 244109.
(38) Zgid, D.; Nooijen, M. *J. Chem. Phys.* **2008**, *128*, No. 014107.
(39) Zgid, D.; Nooijen, M. *J. Chem. Phys.* **2008**, *128*, No. 144116.
(40) Marti, K. H.; Ondík, I. M.; Moritz, G.; Reiher, M. *J. Chem. Phys.* **2008**, *128*, No. 014104.
(41) Kurashige, Y.; Yanai, T. *J. Chem. Phys.* **2009**, *130*, No. 234114.
(42) Ghosh, D.; Hachmann, J.; Yanai, T.; Chan, G. K. *J. Chem. Phys.* **2008**, *128*, No. 144117.
(43) Yanai, T.; Kurashige, Y.; Ghosh, D.; Chan, G. K. *Int. J. Quantum Chem.* **2009**, *109*, 2178−2190.
(44) Lan, T. N.; Kurashige, Y.; Yanai, T. *J. Chem. Theory Comput.* **2014**, *10*, 1953−1967.
(45) Knecht, S.; Legeza, Ö.; Reiher, M. *J. Chem. Phys.* **2014**, *140*, No. 041101.
(46) Moritz, G.; Wolf, A.; Reiher, M. *J. Chem. Phys.* **2005**, *123*, No. 184105.
(47) Nakajima, T.; Hirao, K. *J. Chem. Phys.* **2000**, *113*, 7786−7789.
(48) Wolf, A.; Reiher, M.; Hess, B. A. *J. Chem. Phys.* **2002**, *117*, 9215−9226.

(49) Barysz, M.; Sadlej, A. J. *J. Chem. Phys.* **2002**, *116*, 2696−2704.
(50) Reiher, M.; Wolf, A. *J. Chem. Phys.* **2004**, *121*, 2037−2047.
(51) Reiher, M.; Wolf, A. *J. Chem. Phys.* **2004**, *121*, 10945−10956.
(52) Peng, D.; Hirao, K. *J. Chem. Phys.* **2009**, *130*, No. 044102.
(53) Fukuda, R.; Hada, M.; Nakatsuji, H. *J. Chem. Phys.* **2003**, *118*, 1015−1026.
(54) Fukuda, R.; Hada, M.; Nakatsuji, H. *J. Chem. Phys.* **2003**, *118*, 1027−1035.
(55) Seino, J.; Hada, M. *J. Chem. Phys.* **2010**, *132*, No. 174105.
(56) Melo, J. I.; de Azúa, M. C. R.; Peralta, J. E.; Scuseria, G. E. *J. Chem. Phys.* **2005**, *123*, No. 204112.
(57) Mastalerz, R.; Lindh, R.; Reiher, M. *Chem. Phys. Lett.* **2008**, *465*, 157−164.
(58) Bučinský, L.; Biskupič, S.; Jayatilaka, D. *J. Chem. Phys.* **2010**, *133*, No. 174125.
(59) Neese, F.; Wolf, A.; Fleig, T.; Reiher, M.; Hess, B. A. *J. Chem. Phys.* **2005**, *122*, No. 204107.
(60) Mastalerz, R.; Barone, G.; Lindh, R.; Reiher, M. *J. Chem. Phys.* **2007**, *127*, No. 074105.
(61) Yoshizawa, T.; Hada, M. *Chem. Phys. Lett.* **2008**, *458*, 223−226.
(62) Seino, J.; Uesugi, W.; Hada, M. *J. Chem. Phys.* **2010**, *132*, No. 164108.
(63) Van Zee, R.; Li, S.; Hamrick, Y.; Weltner, W., Jr. *J. Chem. Phys.* **1992**, *97*, 8123−8129.
(64) Hayton, L. J.; Mile, B.; Timms, P. L. *Phys. Chem. Chem. Phys.* **2002**, *4*, 5739−5743.
(65) Wolf, A.; Reiher, M. *J. Chem. Phys.* **2006**, *124*, No. 064102.
(66) Kutzelnigg, W. *Theor. Chim. Acta* **1988**, *73*, 173−200.
(67) Neyman, K. M.; Ganyushin, D. I.; Matveev, A. V.; Nasluzov, V. A. *J. Chem. Phys. A* **2002**, *106*, 5022−5030.
(68) Malkin, I.; Malkina, O. L.; Malkin, V. G.; Kaupp, M. *J. Chem. Phys.* **2005**, *123*, No. 244103.
(69) Autschbach, J. *ChemPhysChem* **2009**, *10*, 2274−2283.
(70) Visscher, L.; Dyall, K. G. *At. Data Nucl. Data Tables* **1997**, *67*, 207−224.
(71) Widmark, P.-O.; Malmqvist, P.-Å.; Roos, B. O. *Theor. Chim. Acta* **1990**, *77*, 291−306.
(72) Widmark, P.-O.; Persson, B. J.; Roos, B. O. *Theor. Chim. Acta* **1991**, *79*, 419−432.
(73) Balasubramanian, K.; Liao, D. W. *J. Phys. Chem.* **1988**, *92*, 6259−6264.
(74) Perdew, J. P.; Yue, W. *Phys. Rev. B* **1986**, *33*, 8800−8802.
(75) Becke, A. D. *Phys. Rev. A* **1988**, *38*, 3098−3100.
(76) Valiev, M.; Bylaska, E.; Govind, N.; Kowalski, K.; Straatsma, T.; Dam, H. V.; Wang, D.; Nieplocha, J.; Apra, E.; Windus, T.; de Jong, W. *Comput. Phys. Commun.* **2010**, *181*, 1477−1489.
(77) Neese, F. *WIREs: Comput. Mol. Sci.* **2012**, *2*, 73−78.
(78) Wessel, G.; Lew, H. *Phys. Rev.* **1953**, *92*, 641−646.
(79) Knight, L. B., Jr.; Cobranchi, S.; Herlong, J.; Kirk, T.; Balasubramanian, K.; Das, K. *J. Chem. Phys.* **1990**, *92*, 2721−2732.
(80) Zhang, Z.; Pyper, N. *Mol. Phys.* **1988**, *64*, 963−981.